












# Early Cardiac Mitochondrial Molecular and Functional Responses to Acute Anthracycline Treatment in Wistar Rats

Gonçalo C. Pereira <sup>\*,1,2</sup> Susana P. Pereira <sup>\*,3</sup> Francisco B. Pereira <sup>†,‡</sup> Nuno Lourenço <sup>†</sup> José A. Lumini <sup>§,¶,||</sup> Claudia V. Pereira <sup>\*,4</sup> James A. Bjork,<sup>|||</sup> José Magalhães <sup>§</sup> António Ascensão <sup>§</sup> Mariusz R. Wieckowski <sup>|||</sup>, António J. Moreno <sup>\*,#</sup> Kendall B. Wallace,<sup>|||</sup> and Paulo J. Oliveira <sup>\*</sup>

<sup>\*</sup>CNC – Center for Neuroscience and Cell Biology, University of Coimbra, UC-Biotech, Cantanhede, Portugal; <sup>†</sup>Centre for Informatics and Systems, University of Coimbra, Polo II, Pinhal de Marrocos, Coimbra, Portugal; <sup>‡</sup>Coimbra Polytechnic – ISEC, Coimbra, Portugal; <sup>§</sup>Health and Leisure, Faculty of Sport Sciences, University of Porto, Research Centre in Physical Activity, Porto, Portugal; <sup>¶</sup>Faculty of Health Sciences, University of Fernando Pessoa, Porto, Portugal; <sup>||</sup>LABIOMEPE – Porto Biomechanics Laboratory, Porto University, Porto, Portugal; <sup>|||</sup>Department of Biomedical Sciences, University of Minnesota Medical School, Duluth, Minnesota; <sup>|||</sup>Nencki Institute of Experimental Biology, Warsaw, Poland; and <sup>#</sup>Department of Life Sciences, University of Coimbra, Coimbra, Portugal

<sup>1</sup>To whom correspondence should be addressed at School of Biochemistry, University Walk, University of Bristol, Bristol BS8 1TD, UK. E-mail: g.pereira@bristol.ac.uk

<sup>2</sup>Present address: School of Biochemistry, University Walk, University of Bristol, Bristol, UK.

<sup>3</sup>Present address: Research Centre in Physical Activity Health and Leisure (CIAFEL), Faculty of Sports, University of Porto, Porto, Portugal.

<sup>4</sup>Present address: University of Miami Miller School of Medicine, Neurological Research Building, Miami, Florida.

## ABSTRACT

Doxorubicin (DOX) is an anticancer drug widely used to treat human and nonhuman tumors but the late and persistent cardio-toxicity reduces the therapeutic utility of the drug. The full mechanism(s) of DOX-induced acute, subchronic and delayed toxicity, which has a preponderant mitochondrial component, remains unclear; therefore, it is clinically relevant to identify early markers to identify patients who are predisposed to DOX-related cardiovascular toxicity. To address this, Wistar rats (16 weeks old) were treated with a single DOX dose (20 mg/kg, i.p.); then, mRNA, protein levels and functional analysis of mitochondrial endpoints were assessed 24 h later in the heart, liver, and kidney. Using an exploratory data analysis, we observed cardiac-specific alterations after DOX treatment for mitochondrial complexes III, IV, and preferentially for complex I. Conversely, the same analysis revealed complex II alterations are associated with DOX response in the liver and kidney. Interestingly, H<sub>2</sub>O<sub>2</sub> production by the mitochondrial respiratory chain as well as loss of calcium-loading capacity, markers of subchronic toxicity, were not reliable indicators of acute DOX cardiotoxicity in this animal model. By using sequential principal component analysis and feature correlation analysis, we demonstrated for the first time alterations in sets of transcripts and proteins, but not functional measurements, that might serve as potential early acute markers of cardiac-specific mitochondrial toxicity, contributing to explain the trajectory of DOX cardiac toxicity and to develop novel interventions to minimize DOX cardiac liabilities.

**Key words:** doxorubicin; animal study; cardiotoxicity; mitochondrial permeability transition; principal component analysis; feature correlation analysis.

Doxorubicin (DOX) is an anthracycline antibiotic that is widely used as a chemotherapeutic agent to treat multiple types of cancers (Simunek *et al.*, 2009; Sterba *et al.*, 2013); however, its therapeutic utility is limited due to the development of a cumulative and dose-dependent cardiotoxicity (Wallace, 2007). Congestive heart failure after DOX treatment is a pressing concern. The mortality observed after a chronic treatment can be as high as 50% (Chatterjee *et al.*, 2010), increasing significantly for cumulative doses higher than 500 mg/m<sup>2</sup> as reported by Singal and Iliskovic (1998). This life-time cumulative dose is equivalent to 13.5 mg/kg<sub>humans</sub> or 83.8 mg/kg<sub>rats</sub>, using reference values and calculations suggested by Nair and Jacob (2016). The etiology of DOX-induced cardiotoxicity is commonly ascribed to a redox-cycling of the drug on complex I of the mitochondrial respiratory chain (Davies and Doroshov, 1986). Reactive oxygen species (ROS) generated during this process are believed to be responsible for the toxic effects on cardiac mitochondria, resulting in impaired oxidative phosphorylation (Santos *et al.*, 2002), loss of mitochondrial calcium homeostasis (Zhou *et al.*, 2001a), and increased apoptotic signaling (Childs *et al.*, 2002). DOX cardiotoxicity can present distinct phenotypes depending on the time elapsed since the initial treatment. Among the wide range of treatment protocols used in different laboratories (Ascensao *et al.*, 2012; Hayward and Hydock, 2007; Solem *et al.*, 1996; Zhou *et al.*, 2001c), we have previously demonstrated that treating Wistar rats with DOX resulted in toxicity only in the cardiac tissue and more easily detected in a subchronic treatment protocol (Pereira *et al.*, 2012).

A distinguishing feature is the fact that DOX toxicity presents a delayed component, manifesting itself years or even decades after treatment (Steinherz *et al.*, 1991). Despite the abundant research in the last decades, the mechanism(s) underlying delayed DOX cardiac toxicity evolution are still far from being understood. Regardless the mechanism(s), it is clinically relevant to identify early signs of specific metabolic or transcriptional alterations observed after acute DOX treatment that may be considered early stress response(s). For this objective, we measured 3 distinct sets of data on cardiac, renal, and hepatic tissue in a rat model subjected to an acute DOX treatment (Ascensao *et al.*, 2012; Pereira *et al.*, 2012):

- i. mRNA and protein levels of subunits of the mitochondrial respiratory complexes (I–IV), ATP synthase, and other relevant mitochondrial components (Cyt c, ANT, VDAC), and applied a suite of exploratory data analysis tools in clusters of transcripts related to the same complex. From this use, we seek to obtain evidence of DOX-induced acute alterations that are present even in the absence of significant differences in the overall respiration flux (Pereira *et al.*, 2016).
- ii. hydrogen peroxide (H<sub>2</sub>O<sub>2</sub>) production by the mitochondrial respiratory chain.
- iii. the sensitivity to the mitochondrial permeability transition (mPTP) as a surrogate of DOX response.

Since the latter markers have both been detected in subchronic DOX toxicity animal models (Cappetta *et al.*, 2017; Zhou *et al.*, 2001c), our objective was to measure similar alterations in the acute model, with the novelty of performing experiments with both complex I and II substrates.

We used in this study a Wistar rat-based animal model and the acute treatment protocol previously described (Pereira *et al.*, 2012). A single dose of 20 mg/kg DOX caused an increase in circulating troponin I and a ~7.6% decrease in cardiac mass with no visible alterations on the mitochondrial functional parameters evaluated. However, if a similar dosage was spanned over the period of 7 weeks (subchronic model), a clear mitochondrial impairment was observed (Pereira *et al.*, 2012; Zhou *et al.*, 2001a, b, c), suggesting that DOX acute effects may progress into mitochondrial bioenergetic dysfunction. Moreover, it also suggests that the acute DOX toxicity model may be used to assess mitochondrial alterations that precede functional changes. Therefore, we included mitochondrial molecular parameters in the present study and anticipated that our novel approach will allow the assessment of early markers of acute DOX cardiotoxicity, facilitating the development of biomarkers to be used in the clinic for timely identification of patients with higher susceptibility to latent DOX toxicity and for the development of interventions aimed at decreasing DOX off-target cardiac toxicity.

## MATERIALS AND METHODS

**Reagents.** DOX hydrochloride, (7S, 9S)-7-[(2R, 4S, 5S, 6S)-4-amino-5-hydroxy-6-methyloxan-2-yl]oxy-6, 9, 11-trihydroxy-9-(2-hydroxyacetyl)-4-methoxy-8, 10-dihydro-7H-tetracene-5, 12-dione hydrochloride, chemical purity ≥ 98%, was obtained from Sigma-Aldrich (Barcelona, Spain) and prepared in a sterile saline solution, NaCl 0.9% (pH 3.0, HCl) and stored at 4°C for no longer than 5 days upon rehydration. All other chemicals were of the highest commercially available grade of purity. Aqueous solutions were prepared in ultrapure (type I) water (Milli-Q Biocel A10 with pretreatment via Elix 5, Millipore, Billerica, Massachusetts). For nonaqueous solutions, ethanol (99.5%) or dimethylsulfoxide (DMSO), both from Sigma-Aldrich, was used as solvent.

**Animal care.** Animal handling was performed in accordance with the European Convention for the Protection of Vertebrate Animals used for Experimental and Other Scientific Purposes (CETS no.123) and Portuguese rules (DL 129/92). The procedures were approved by the CNC Committee for Animal Welfare and Protection. Animal handlers and the authors G.C.P., S.P.P., J.M., A.A., and P.J.O. are credited by the European Federation for Laboratory Animal Research (FELASA) category C for animal experimentation (accreditation no. 020/08).

Male Wistar rats, CrI: WI(Han), were purchased from Charles River (France) with 14 weeks of age, acclimated for 10–14 days prior to the initiation of experiments and maintained in the local animal house facility (CNC—School of Medicine, University of Coimbra, Coimbra, Portugal). Animals were group-housed in type III-H cages (Tecniplast, Italy) with irradiated corn cob grit bedding (Scobis Due, Mucedola, Italy) and environmental enrichment and under controlled environmental requirements (22°C, 45%–65% humidity, 15–20 air changes/h, 12 h artificial light/dark cycle, noise level < 55 dB) and free access to standard rodent food (4RF21 GLP certificate, Mucedola, Italy) and acidified water (at pH 2.6 with HCl) *ad libitum*.

The experimental model was performed as previously described (Pereira et al., 2012). Briefly, male Wistar-Han rats ( $N = 34$ ) were randomly divided into 2 groups ( $n = 17$  each group) and received a single intraperitoneal injection (i.p.) of DOX (20 mg/kg of body weight) or an equivalent volume of vehicle solution (NaCl 0.9% pH 7, controls), 24 h before sacrifice.

All animals were injected during the light phase of the cycle and weighed at the beginning and end of the experimental treatment period (data available in Pereira et al. [2012]). Non-fasted animals were euthanized in pairs by cervical dislocation followed by decapitation, to confirm death and exsanguination. Organs were immediately extracted from the body and quickly washed in appropriate ice-cold buffer before being weighed (data available in Pereira et al. [2012]). Tissues intended for mRNA and protein analyses were stored separately in RNAlater (Applied Biosystems/Ambion, Austin, Texas) at  $-80^{\circ}\text{C}$ , accordingly to manufacturer guidelines.

**Isolation of mitochondrial fraction.** Mitochondria were isolated by a standard procedure currently used in our laboratory (Pereira et al., 2012). Briefly, organs were excised and finely minced in ice-cold isolation medium containing 250 mM sucrose, 10 mM HEPES, 1 mM ethylene glycol tetraacetic acid (EGTA), and 0.1% defatted BSA (pH 7.4, KOH). After washing the blood, organs were homogenized with a motor-driven Teflon Potter homogenizer. For the isolation of cardiac mitochondrial fractions, isolation medium was supplemented with 0.5  $\mu\text{g}/\text{ml}$  of protease (Subtilisin A, Type VIII from *Bacillus licheniformis*, Sigma-Aldrich, Madrid, Spain). Protease was removed from the cardiac homogenate by centrifugation at  $14\,400 \times g$  for 10 min at  $4^{\circ}\text{C}$  and the pellet, essentially devoid of protease, was gently homogenized and resuspended to its original volume with a loose-fitting homogenizer. Subsequently, all homogenates were centrifuged at  $750 \times g$  for 10 min at  $4^{\circ}\text{C}$  and the resulting supernatants at  $10\,000 \times g$  for 10 min. Mitochondrial pellet was resuspended using a paintbrush and centrifuged twice at  $10\,000 \times g$  for 10 min before obtaining a pure mitochondrial suspension. EGTA and defatted BSA were omitted from the final washing medium (pH 7.2, KOH). Mitochondrial protein was quantified by the biuret method using bovine serum albumin (BSA) as standard. Mitochondrial preparations were kept on ice during experiments, which were carried out after 20 min recovery period and within 5 h. The respiratory control ratio values of the mitochondrial preparations were within the standard range, demonstrating a good coupling between respiration and ATP phosphorylation (heart saline glutamate plus malate  $4.6 \pm 0.4$ , succinate  $2.7 \pm 0.2$ ; liver saline glutamate plus malate  $9.5 \pm 1.0$ , succinate  $8.2 \pm 1.5$ ; kidney saline glutamate plus malate  $4.1 \pm 0.3$ , succinate  $3.5 \pm 0.2$ ; there was no statistical difference between saline vs. DOX group), previously reported in Pereira et al. (2012).

**Measurement of hydrogen peroxide.**  $\text{H}_2\text{O}_2$  generation was measured fluorimetrically using a modified method previously described by Barja (2002). Briefly, the method consists in the use of homovanillic acid which reacts with  $\text{H}_2\text{O}_2$  in the presence of horseradish peroxidase to form the fluorescent dimer 2,2'-dihydroxy-3,3'-dimethoxydiphenyl-5,5'-diacetic acid ( $\lambda_{\text{Ex}}/\lambda_{\text{Em}} = 312/420 \text{ nm}$ ). Reactions (500  $\mu\text{l}$ ) were conducted in standard glass test tubes under constant magnetic stirring and incubated in a water bath at  $30^{\circ}\text{C}$ . Small volumes of reactants were combined in the following order to pre-added incubation medium (145 mM KCl, 30 mM Hepes [pH 7.4, KOH], 5 mM  $\text{KH}_2\text{PO}_4$ , 3 mM  $\text{MgCl}_2$ , 100  $\mu\text{M}$  EGTA, 0.1% fatty acid-free albumin) to reach the

following concentrations: 0.125  $\mu\text{g}$  mitochondrial protein, 6 U/ml horseradish peroxidase, and 100  $\mu\text{M}$  homovanillic acid.  $\text{H}_2\text{O}_2$  production was determined in mitochondria energized with 5 mM glutamate/malate or 5 mM succinate. At these concentrations,  $\text{H}_2\text{O}_2$  production is not substrate dependent. In some experiments, specific inhibitors for complex I (rotenone, 1  $\mu\text{M}$ ) or for complex III (antimycin A, 0.5  $\mu\text{M}$ ) were used in combination with respiratory substrates to block electron transport and maximize  $\text{H}_2\text{O}_2$  production. Arbitrary fluorescence units were converted to nmol  $\text{H}_2\text{O}_2$  by extrapolation through a standard curve established by addition of known amounts of  $\text{H}_2\text{O}_2$  in the presence of horseradish peroxidase and homovanillic acid. Values were then normalized to protein amount and expressed as nmol  $\text{H}_2\text{O}_2/15 \text{ min}/\text{mg}$  protein.

**Mitochondrial calcium accumulation.** Extramitochondrial free  $\text{Ca}^{2+}$  was assayed by monitoring the variations in fluorescence of the hexapotassium salt of the probe Calcium Green 5-N (Ca5GN; Invitrogen, Spain, C-3737), which increases its yield upon binding to calcium, and as previously described (Rajdev and Reynolds, 1993). Briefly, isolated mitochondrial fraction (0.25 mg/ml cardiac, 0.75 mg/ml liver and kidney) were suspended in 2 ml of buffer containing 200 mM sucrose, 10 mM Tris, 10  $\mu\text{M}$  EGTA (to complex basal calcium), 5 mM  $\text{KH}_2\text{PO}_4$  for cardiac mitochondria, or 1 mM  $\text{KH}_2\text{PO}_4$  for liver and kidney mitochondria, combined with 812 nM of Ca5GN. After mitochondrial energization with 2.5 mM glutamate plus malate (enabling mitochondrial energization through complex I) or 2.5 mM succinate in the presence of 1  $\mu\text{M}$  rotenone (enabling mitochondrial energization through complex II) a baseline of 60 s was obtained before the addition of a single pulse of calcium of 65–100, 50–100, and 40–65 nmol for heart, liver, and kidney mitochondria. Fluorescence was continuously recorded in a water-jacketed cuvette holder at  $30^{\circ}\text{C}$  using a PerkinElmer LS-55 fluorescence spectrometer (PerkinElmer Life and Analytical Sciences, Boston, Massachusetts) at  $\lambda_{\text{Ex}}/\lambda_{\text{Em}} = 506/531 \text{ nm}$ . Five-nanometer slits were used for excitation and emission wavelengths. Adequate controls were performed to assess possible interferences in probe fluorescence, under either low or high calcium concentrations (no interferences were observed for the experimental conditions described). Possible interferences with DOX were discarded since its emission peaks at 550 nm, a higher wavelength than our emission filter; and, excitation peaks at 475 nm, meaning that only a small fraction of the drug could lower Ca5GN excitation at 506 nm. Cyclosporin A (CsA), a desensitizer of the mPTP (Broekemeier et al., 1989), was used to confirm that the recorded event was related to the mPTP.

**Calcium-induced mitochondrial swelling.** Mitochondrial osmotic volume changes associated with the calcium-induced mPTP were assessed by turbidimetry (Halestrap and Davidson, 1990). The optical density was monitored at 540 nm with a Jasco V-560 spectrophotometer (Jasco Inc., Easton, Maryland) equipped with a magnetic stirrer and a water-jacketed cuvette holder connected to a water bath set to  $30^{\circ}\text{C}$ . The assay was carried out in the same buffer as described above for calcium loading experiments, but at a protein concentration of 0.5 mg/ml (heart) or 1.0 mg/ml (liver and kidney) was used. After a 60 s baseline, a single pulse of calcium of 20–50 nmol/mg protein or 10–50 nmol/mg protein was added to heart or liver and kidney mitochondria, respectively. Absorbance variations were recorded and analyzed with the manufacturer's software. The swelling amplitude presented in the graphs is defined as the difference in absorbance between the time-point that corresponds to half

of the maximum swelling amplitude of the control record and the baseline before calcium addition (larger values mean greater sensitivity to mPTP). CsA was used to confirm that the recorded events were related to the mPTP.

**Total RNA isolation.** RNA was isolated using the RNeasy Mini Kit (Qiagen Inc., Valencia, California). Briefly, 20 mg of each RNAlater-conserved frozen tissue was thawed and ground in a glass pestle homogenizer followed by further homogenization with a 27-gauge needle connected to a syringe. The purification was performed as described in the manufacturer's RNA cleanup protocol, following its suggestions. RNA was quantified using a NanoDrop spectrophotometer (ThermoFisher Scientific Inc., Rockford, Illinois). RNA quality and purity were assessed by observing a spectral scan with a single prominent A260 peak and A260/A280 ratio greater than 2.

**Protein extraction and western blot.** RNAlater-conserved frozen tissue (70–150 mg) was thawed and ground in a glass pestle homogenizer in a 10% (m/v) RIPA buffer (150 mM NaCl, 50 mM Tris, pH 8.8, 0.5% sodium deoxycholate, 0.1% SDS, and 1% Igepal), supplemented with 5  $\mu$ l/mg of tissue of protease inhibitors cocktail (P8340, Sigma-Aldrich Inc., St. Louis, Missouri). The homogenate was then centrifuged at 14,000  $\times$  g for 5 min to remove cellular debris. Protein concentration was determined by BCA Protein Assay Kit (Thermo Fisher Scientific Inc.) using BSA as standard. Extracted proteins were diluted in Laemmli buffer (BioRad Laboratories, Hercules, California) supplemented with 2%  $\beta$ -mercaptoethanol then boiled at 95°C for 5 min. Equal amounts of protein (25  $\mu$ g) were loaded into 12% polyacrylamide gels separated by SDS-PAGE. Then, proteins were transferred to PVDF membranes (Millipore) at 100 V for 90 min, at 4°C. Membranes were blocked with 0.25% of skimmed dry milk in Tris-buffered saline (154 mM NaCl, 50 mM Tris, pH 8.0) containing 0.1% Tween-20 (TBS-T) using the SNAP-id system (Millipore) with 10 min incubation. After washing twice with TBS-T in the same system, membranes were incubated with primary antibody directed against the respective protein (listed in [Supplementary Table 1](#)) through traditional procedures, overnight at 4°C. After washing twice in the SNAP-id system, membranes were incubated in this system with the respective alkaline phosphatase-linked secondary antibody (1:6000), prepared in TBS-T. The membranes were processed for protein detection using the Enhanced Chemi-Fluorescence system (GE Healthcare, Buckinghamshire, UK) and imaged with the Versa Doc imaging system (BioRad). The densities of each band were calculated with Quantity One Software (BioRad) and expressed as a percentage of control. The assay was standardized by reprobating the membranes for actin (#MAB1501, Millipore) immunoreactivity (1:10,000) to verify whether similar amounts of protein present in all lanes.

**Real time qRT-PCR.** cDNA was synthesized from extracted RNA (0.5–1.5  $\mu$ g) using random primers along with the Omniscript Reverse Transcription Kit (Qiagen). All primers ([Supplementary Table 2](#)) used for real time qRT-PCR were designed using the web-based PrimerQuest software (Integrated DNA Technologies, Inc., Coralville, Iowa). Real time qRT-PCR was carried out using FastStart SYBR Green I Kit (Roche Diagnostics, Indianapolis, Indiana) with 10  $\mu$ l reaction volume and performed in a LightCycler (Roche Diagnostics). Quantitation of gene expression was achieved by measuring target messenger RNA (mRNA) copy number against a 10-fold serial dilution of target-specific DNA standard ranging between 10<sup>7</sup> and 10<sup>3</sup> DNA copies. A target-specific DNA standard was prepared for each

transcript by performing a 150  $\mu$ l PCR reaction using HotstarTaq PCR Master Mix Kit (Qiagen) and cleaning the product using the Qiaquick PCR Purification Kit (Qiagen). The purified DNA standard was visualized by running a 100 ng aliquot on a 1.5% agarose gel and verifying that a single product of the proper size was present. The DNA standard was quantified spectrophotometrically using the NanoDrop ND1000 and diluted to a standard stock concentration of 5  $\times$  10<sup>9</sup> DNA copies per microliter. 18S ribosomal RNA was used to normalize gene expression. Real-time qRT-PCR of control and treated samples for each gene was performed on the same run to minimize potential run to run variability.

**Exploratory analysis and data statistical analysis.** Results are shown as means  $\pm$  SEM of the indicated number of experiments. Statistical significance between mean differences was determined using 2-tailed Student's t-test after normality and homogeneity of variances was assessed using a Shapiro-Wilk and Levene's test. Control group was matched against the treated group for each day to exclude the variability associated with mitochondrial isolation. In the specific case when seeking to ascertain whether changes between saline and DOX group in the heart are actually different from changes in other tissues, regardless of the intertissue baseline (ie, for mRNA) data were analyzed by a 2-way ANOVA with planned contrasts against the interaction between treatment and tissue so that significant relative changes (fold-change) are dependent on tissue. *p*-Values were thereafter adjusted for multiplicity using Šidák post hoc test. Differences were considered significant if *p* < .05 and categorized accordingly to their interval of confidence. Statistical analyses were performed using Graph Pad Prism version 5.0 (GraphPad Software, Inc., San Diego, California), except of the 2-way ANOVA, which was performed using JMP-SAS version 9.03 (SAS Campus Drive, Cary, NC).

The exploratory analysis comprises the application of feature correlation analysis (FCA) and principal component analysis (PCA) methods. For both studies, samples with missing values were discarded. Standardization was applied to all the remaining features and the corresponding standard scores were used. FCA was performed using the Pearson correlation coefficients, whose values belong to the interval [–1, +1]: +1 signals a total positive linear correlation, 0 identifies no linear correlation and –1 refers to a total negative linear correlation. To simplify the analysis of the results, we consider just the absolute magnitude of change and created several graphical displays of the correlation matrices.

PCA was applied to find the 2 principal components that collectively explain most of the variability of the original set. The obtained eigenvectors were used to project the original samples in a set of 2D plots. Both FCA and PCA studies were performed using Python2, version 7. We relied on the Pandas package to load, store and transform the data (McKinney, 2010). The statistical analysis was performed using SciPy (Jones et al., 2001) and scikit-learn (Fabian Pedregosa et al., 2011). FCA correlation plots were created using Matplotlib and Biokit modules (Hunter, 2007). PCA scatter plots and density region charts were obtained with Orange Biolab (Demsar et al., 2013).

## RESULTS

### Exploratory Data Analysis

In the present research, we applied PCA and FCA to discover correlations and clustering patterns that help to identify

relevant mitochondrial markers for the early detection of acute DOX toxicity. The small number of available samples prevents a complete and robust statistical analysis of the results. However, PCA provides initial insight regarding the separation of the treatment groups (Saline vs. DOX) allowing the discovery of important relevant trends. The 12 panels from Figure 1 illustrate the separation between Saline and DOX samples, for each of the 4 mitochondrial respiratory complexes in heart, kidney, and liver tissues, respectively. To allow an informative 2D visualization, we considered just the 2 principal components (explaining >70% of the variance) and projected the original data in the lower dimensional space.

Considering the cardiac tissue (Figure 1a), the 4 panels representing each of the respiratory complexes tend to exhibit a clear separation between areas comprising samples from saline (blue area) and DOX-treated rats (red area). The separation is clearly visible for complex I whereas some minor perturbations are observed in complexes II, III, and IV. These minor differences correspond to specific regions where the separation is not evident, suggesting that it might be difficult for a computational analysis to accurately classify examples in these locations. Class separation between treatment groups for some respiratory complexes is also less evident when analyzing the remaining tissues in the study. For example, when analyzing the renal tissue (Figure 1b) a visible class separation in complexes II and III was observed, but the other complexes displayed several mixed subareas that might compromise the correct identification of the samples. Similarly, complex II in the hepatic tissue (Figure 1c) tends to generate a clear boundary between the 2 treatment groups, whereas the other complexes reveal several density subareas.

Overall, PCA analysis of mRNA transcripts identified complex I as preferable target for DOX acute toxicity in the heart whereas complex II preferentially relates to DOX effects in the liver and kidney. Complexes III and IV are not robust markers to differentiate DOX toxicity in the analyzed tissues of this study.

Next, we complemented the PCA with individual FCA, to estimate the dependence that may exist between every pair of features. Our analysis considered all pairwise feature correlations and aimed to identify variables exhibiting high sensitivity to DOX. Figures 2a–c show the global trend in the correlation changes resulting from DOX administration for features describing mRNA and protein levels in the heart, kidney and liver tissues, respectively.

Observationally, there are some noticeable differences in the global patterns shown in Figure 2. In regard to liver (Figure 2c), DOX administration tends to have a minor impact in the correlation strength change (high number of blank cells). Nonetheless, there is a high and consistent change involving the expression of subunit NDUF8 in the liver. Conversely, Figures 2a and 2b, representing heart and kidney, respectively, exhibit a considerable number of filled cells identifying pairs with sizable correlation changes. The correlation change of NDUF8 that was signaled in the liver is also present in these tissues, although to a lesser extent. Regarding features from complex I, some additional correlation changes are observed, namely ND1 and ND2 mRNA in the kidney and ND6 and NDUF54 mRNA in the heart.

In respect to complex II, no noticeable changes in correlation were observed, regardless of the tissue in study. In complex III-related features, DOX treatment showed a stronger effect on the correlation change of CytB mRNA and UQCRFS1 protein levels in kidney. Finally, a few correlation changes regarding complex IV features were also observed in heart and kidney, but not as obvious as reported above (Supplementary Fig. 1).

Overall, the FCA analysis suggests that the impact of the DOX treatment is easier to perceive if considering samples from heart and kidney when compared with liver, in agreement with findings obtained from PCA.

#### Mitochondrial Hydrogen Peroxide Production

DOX-induced oxidative stress is considered a hallmark of its toxicity (Pereira et al., 2012). In the present work, we investigate the contribution of different sites of the mitochondrial respiratory chain to the overall oxidative response by DOX. In respect to complex I-sustained respiration, H<sub>2</sub>O<sub>2</sub> production was similar to control values in heart and kidney mitochondria regardless of the energization conditions tested (Figs. 3a and 3c). However, in liver mitochondria, H<sub>2</sub>O<sub>2</sub> production in the presence of rotenone was higher in mitochondria from DOX-treated animals (11 ± 3%) even though no statistical differences were observed in the presence of antimycin A alone (18 ± 10%) or with antimycin A plus rotenone (1 ± 2%).

When mitochondria were energized with complex II-linked substrates, heart mitochondria from DOX-treated animals showed increased production of H<sub>2</sub>O<sub>2</sub> in the presence of substrate alone, yet it was not statistically significant (164 ± 72%,  $p = .06$ ; Figure 3a). Interestingly, this alteration was only observed in the absence of respiratory chain inhibitors as other conditions were similar to controls, reflecting ROS production through reverse electron transfer.

In regard to liver and kidney, mitochondria from DOX-treated animals energized with complex II-linked substrates presented similar levels of H<sub>2</sub>O<sub>2</sub> production under all tested conditions (Figs. 3b and 3c).

Overall, liver mitochondria from DOX-treated animals appear to generate more H<sub>2</sub>O<sub>2</sub> compared with heart or kidney mitochondria but only when the respiratory chain is challenged by oxidative phosphorylation (OXPHOS) inhibitors, suggesting a higher flux of electrons through the respiratory chain at the complex I level.

#### Mitochondrial Calcium Loading Capacity

To assess mitochondrial calcium handling, we measured the sensitivity of each mitochondrial preparation to undergo the calcium-induced mPTP. Heart mitochondria from DOX-treated animals showed no alteration neither in calcium retention time nor release rate regardless of the respiratory substrate used (Figure 4a). Similarly, no treatment-related effects on calcium flux were observed in kidney mitochondria (Figure 4c). However, liver mitochondria from DOX-treated animals showed an apparent decreased sensitivity to mPTP opening (Figure 4b). Hepatic mitochondrial preparations retained calcium for 43 ± 30% longer with complex I-linked respiration and 36 ± 19% for complex II-linked respiration compared with control group although no statistical significance was observed ( $p = .194$  and  $.098$ , respectively). In addition, calcium release rates were decreased by 49 ± 19% with complex I-linked respiration and 18 ± 27% with complex II-linked respiration. Significance was not always achieved due to the high variability in response to the treatment (Figure 4b). Confirming that all previous mentioned alterations were related to the mPTP opening is the fact that preincubation with CsA, the classic mPTP desensitizer (Broekemeier et al., 1989) prevented calcium release (Table 1).

Additionally, the same mitochondrial preparations were assessed for calcium-induced mitochondrial swelling in similar conditions to those aforementioned. Corroborating the above results, heart mitochondria swelling amplitude and swelling rate were not altered after acute treatment with DOX, regardless

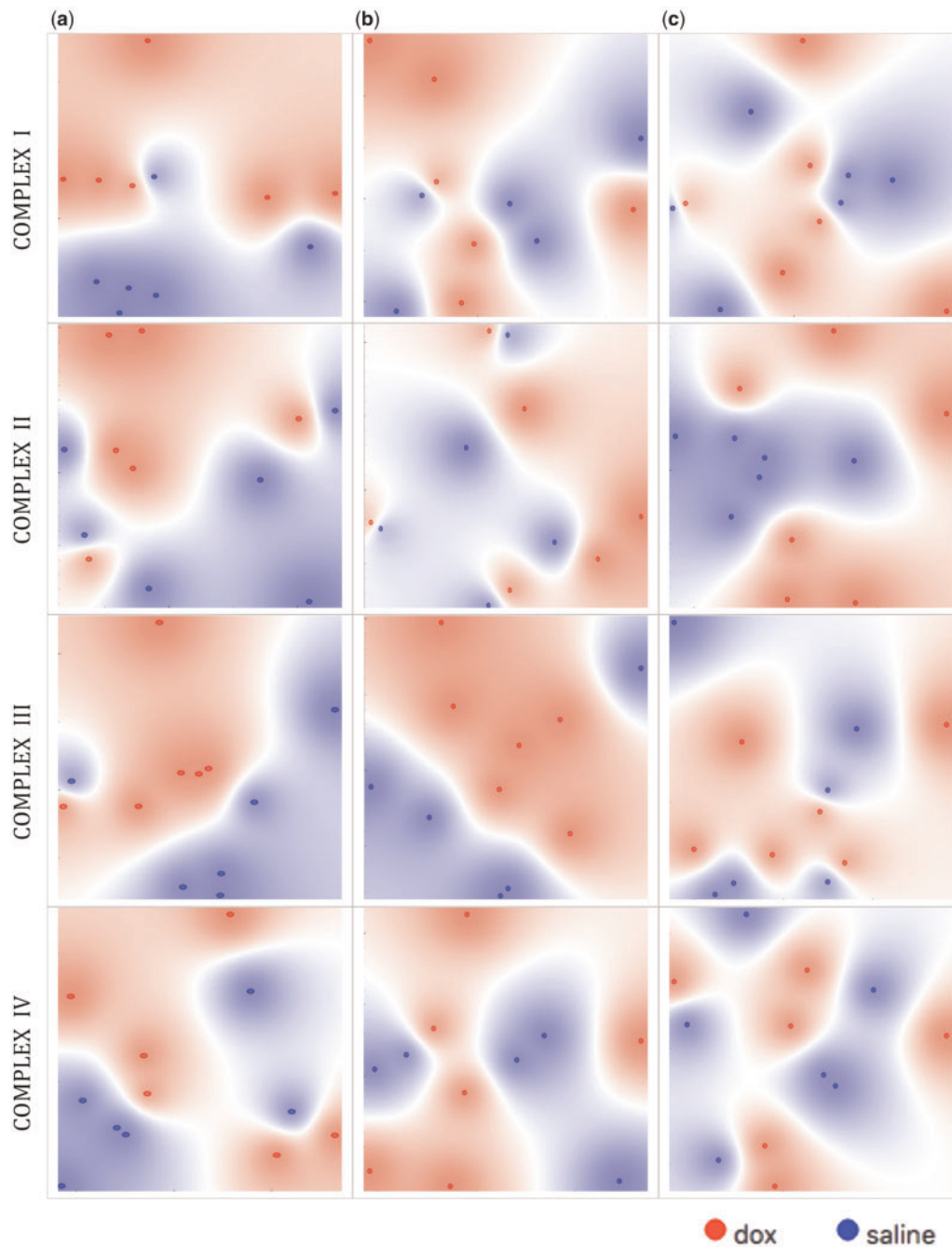


**Figure 1.** PCA projection along the 2 principal components of the separation between DOX (red) and Saline (blue) samples for heart (a), kidney (b), and liver (c). The 2 class density colors identify the area of influence of each group. The 4 panels in each figure display results obtained with each mitochondrial respiratory complex. PCA was performed on transcripts (mRNA) of genes encoding proteins from mitochondrial complexes I-IV. The study was based on 12 samples (6 Saline and 6 DOX) and 13, 4, 6, and 7 transcripts for each one of the 4 respiratory complexes (I-IV), respectively. PCA was performed separately for each combination of tissue and specific respiratory chain complex, to simplify the identification of situations in which a clear boundary between the 2 treatment groups emerges. (For interpretation of the references to colour in this figure legend, the reader is referred to the web version of this article.)

of the respiratory substrate used (Figure 5a). Likewise, in kidney mitochondria, amplitude and swelling rate were not different from control (Figure 5c). However, liver mitochondria from DOX-treated animals appear to have slower swelling rate ( $6 \pm 12\%$  and  $21 \pm 37\%$  for glutamate/malate and succinate, respectively; Figure 5b) despite no apparent change in swelling amplitude ( $20 \pm 30\%$  and  $11 \pm 31\%$  for glutamate/malate and succinate, respectively). As in calcium-loading capacity experiments, a high variability in response to the treatment was observed for liver

mitochondria preventing any statistical differences. CsA under the experimental swelling conditions abolished all the effects, confirming the opening of the mPTP (Table 2).

Two major regulators of the mPTP are: cyclophilin D (Cyp-D) in the matrix and ANT in the inner membrane (Silva et al., 2018). Cyp-D protein levels remained constant after the acute treatment regardless of the tissue analyzed (Table 3). We next measured mRNA and protein content of 2 ANT isoforms (Table 4). The  $40 \pm 6\%$  cardiac-specific decrease of ANT1 mRNA was

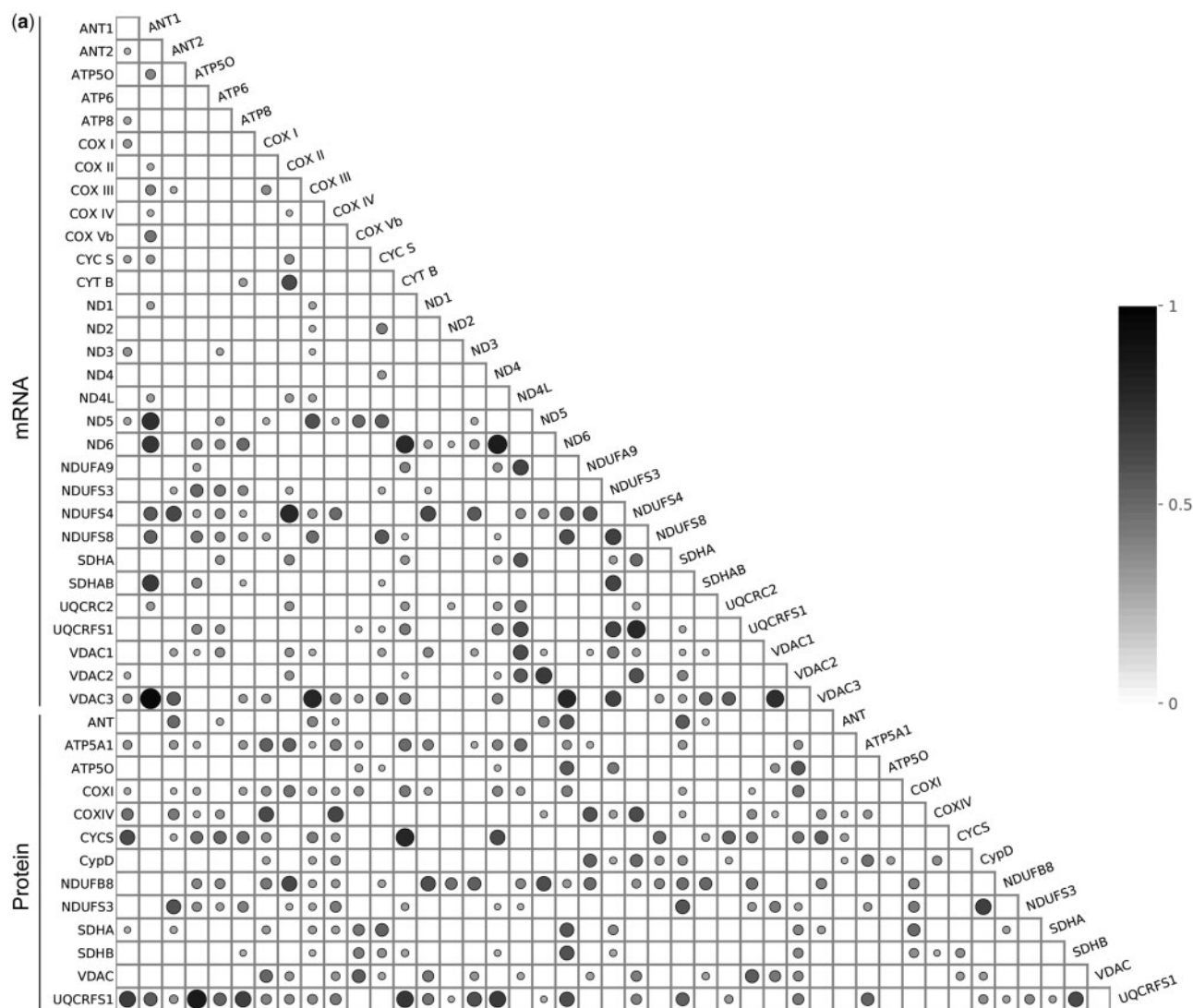


**Figure 2.** Matrices with all correlation changes in the features that result from the administration of DOX: a, heart; b, kidney; c, liver. Blank cells indicate that there is no significant change in correlation levels calculated before and after DOX treatment. Cells with circles identify sizable changes in the correlation value. The area and shading of a circle are directly proportional to the absolute magnitude of change.

significantly stronger than the effects observed in liver and kidney. Similarly, the  $26 \pm 6\%$  decrease of ANT2 mRNA was significant when compared with kidney. Still, no change in protein levels were observed after the 24 h treatment (Table 3). Moreover, no treatment- or tissue-specific effects were detected regarding the protein and mRNA levels of VDAC, a porin of the outer mitochondrial membrane which governs ion and metabolites flux into mitochondria (Table 4).

Overall, the sensitivity to mPTP opening remains constant in heart mitochondria after the acute treatment in contrast with liver mitochondria which show strong resistance to mPTP opening. However, this mPTP modulation cannot be attributed to changes in the protein levels of mPTP-related proteins. We suggest instead that increased electron flux through the respiratory chain in liver mitochondria is modulating mPTP opening.

## DISCUSSION

The mechanisms underlying DOX-selective cardiotoxicity remain undefined. Nevertheless, it is being more widely accepted

that the antitumor activity is independent of cardiac toxicity, which may involve alterations of mitochondrial function (discussed in Pereira et al. [2011]). Acute DOX cardiac toxicity occurs during the early treatment of patients (high dose) and usually include symptoms which are therapeutically easy to manage and resolve once treatment is discontinued (Tokarska-Schlattner et al., 2006). Alternatively, a small, but significant number of patients develop chronic cardiotoxicity that can manifest itself at the end of treatment or several years later (Steinherz et al., 1991). However, unlike acute toxicity, the dose-dependence together with its difficult early detection, renders DOX chronic toxicity life-threatening and largely uncontrolled.

Regardless the mechanism(s) involved in DOX cardiotoxicity, the available data not only demonstrates mitochondrial involvement (Zhou et al., 2001c), but also differences related to each treatment protocol (acute vs. subchronic in Pereira et al. [2012]). Previously, by using Wistar rats treated with a single dose of DOX (20 mg/kg), Ascensao et al. (2006, 2011, 2005) observed that heart mitochondria respiration and

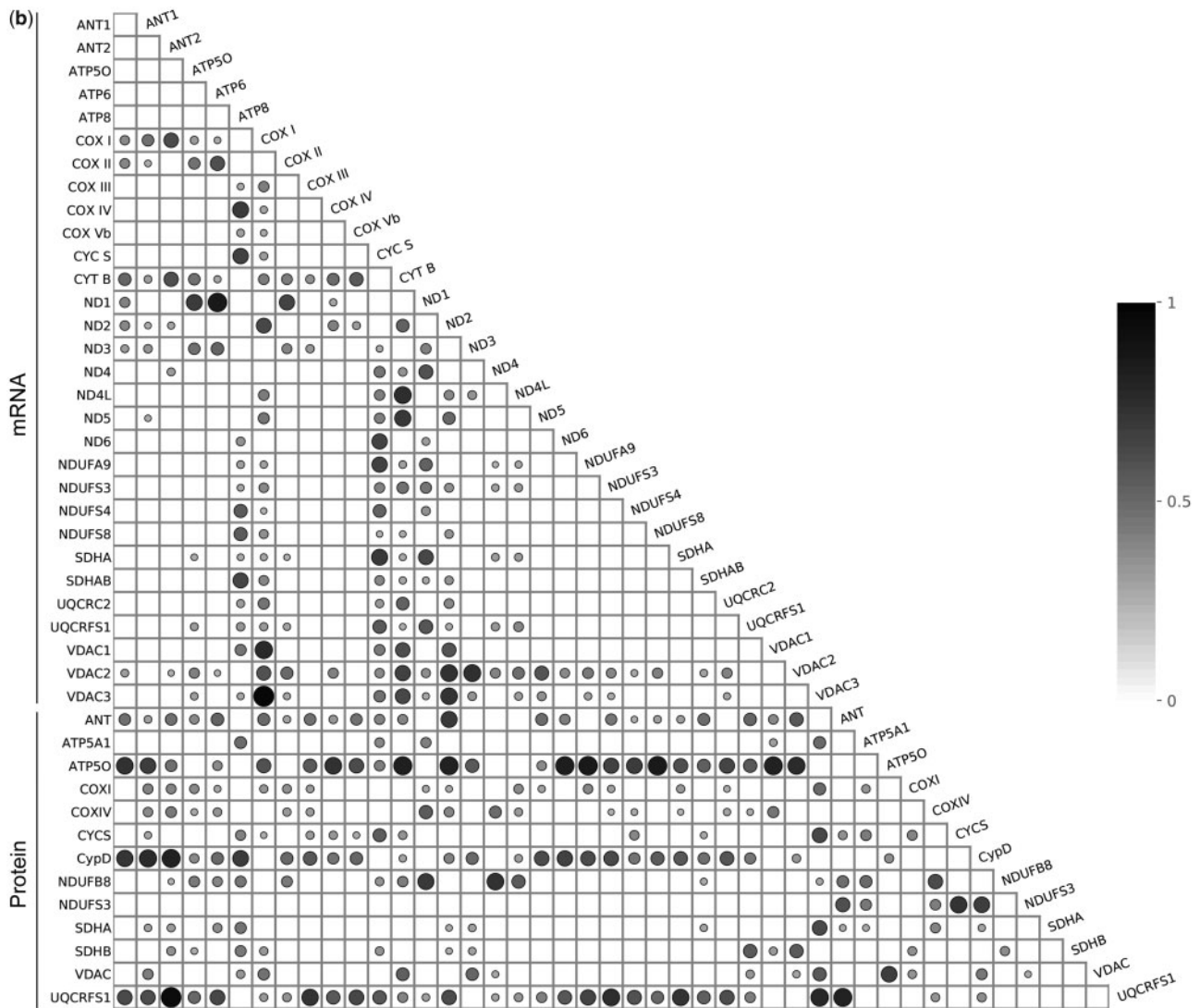


Figure 2. Continued.

phosphorylation capacity were impaired after 24 h treatment. In contrast, we applied the same treatment protocol in younger rats of the same strain and observed no DOX effects on cardiac mitochondrial respiration, although minor, but statistical significant alterations were measured in ADP-stimulated respiration in liver (increase) and kidney (decreased) mitochondria (Pereira et al., 2012), suggesting a differential response to DOX determined by age at time of treatment. Considering that a very large proportion of children with cancer are treated with DOX (van Dalen et al., 2009) despite its potential cardiotoxicity, it is relevant to identify early alterations of mitochondrial parameters/markers, which can be considered as early cardiac-specific stress responses to drug treatment.

It has been demonstrated in different rat models that DOX subchronic treatment causes inhibition of mitochondrial respiration; oxidation of proteins, lipids, and nuclei acids; loss of cardiolipin and, alterations in the antioxidant enzymatic network (Oliveira et al., 2004, 2006; Pereira et al., 2016; Wallace, 1986; Zhou et al., 2001b). Alterations of mitochondrial activity were also reported in different cardiac-like cell models, associated to increased cell death (Asensio-Lopez et al., 2016; Cunha-Oliveira

et al., 2018; Sardao et al., 2009). Taking these subchronic markers of DOX toxicity into account we selected and measured relevant mitochondrial mRNA and protein content, respiratory chain-derived  $H_2O_2$ , and calcium-loading capacity in 16-weeks old Wistar rats, suspecting that they would be reliable markers of DOX acute toxicity.

Our data on calcium-loading capacity suggest that liver mitochondria are resistant to mPTP opening after DOX treatment in agreement with the increased mitochondrial bioenergetics fitness previously described by our lab (Ascensao et al., 2011; Pereira et al., 2012). Similarly, liver mitochondria displayed increased  $H_2O_2$  production when mitochondria were stressed by using OXPHOS inhibitors. Together with the improved mitochondrial fitness previously described, it suggests an increased electron flow through the respiratory chain. Electron flow has also been reported to modulate mPTP sensitivity (Fontaine et al., 1998), corroborating our data from calcium-loading capacity experiments. However, because a single timepoint was evaluated in our experimental setup (24 h), it was not possible to determine if DOX effect in liver mitochondria is slow to develop or long-lasting.



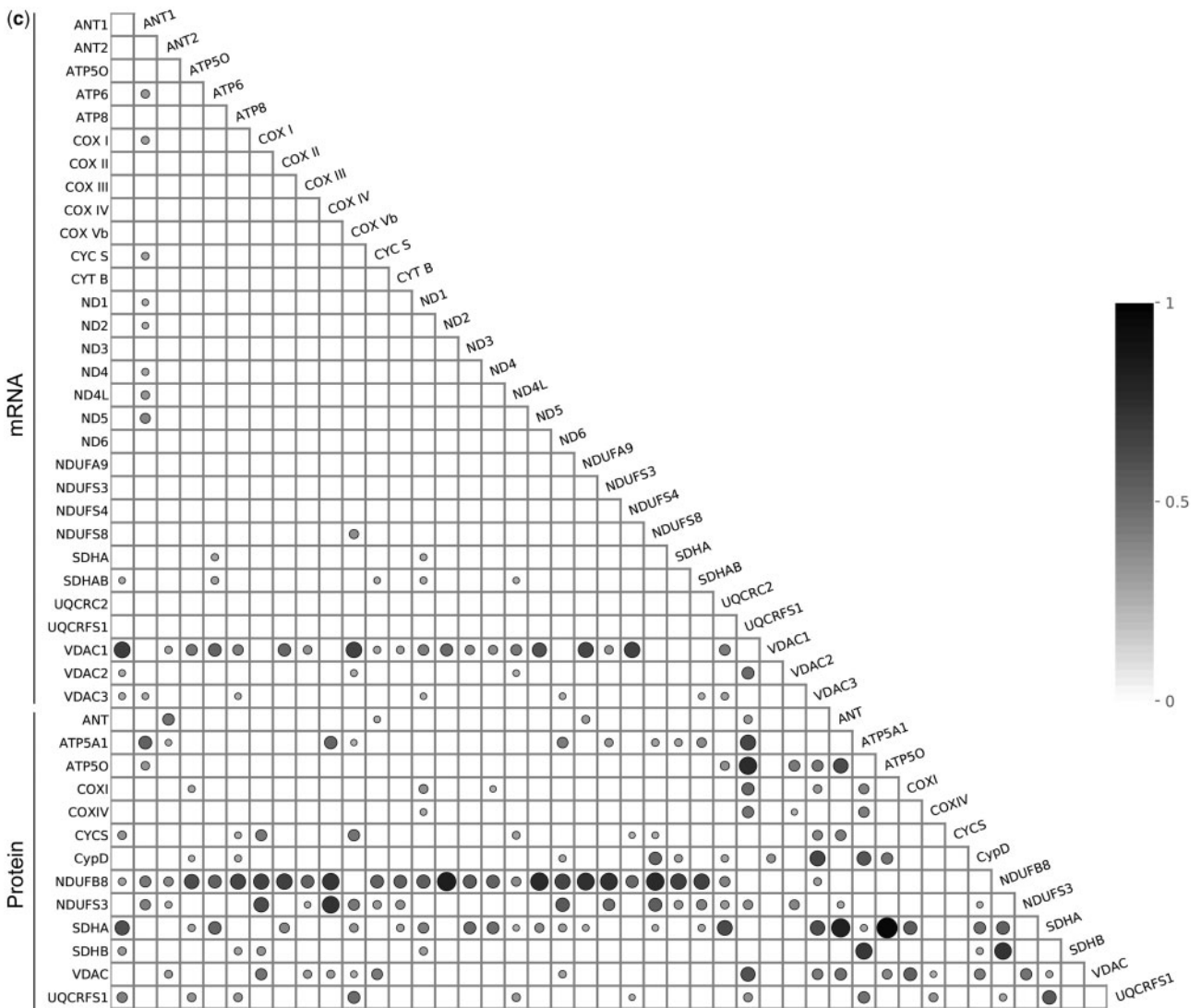


Figure 2. Continued.

Considering that increased mitochondrial oxidative stress and loss of calcium-loading capacity are regarded as hallmarks of chronic DOX-induced cardiac mitochondriopathy (Pereira *et al.*, 2011; Zhou *et al.*, 2001a, b, c), our negative results in respect to cardiac tissue suggest that  $H_2O_2$  generation and early loss of calcium-loading capacity following an acute DOX treatment are not reliable markers for early DOX cardiotoxicity. Therefore, it is relevant to identify alternative mitochondrial markers in order to recognize early functional or molecular signs of DOX-related cardiovascular toxicity.

To this end, we also performed mRNA and protein analysis for components relevant for the maintenance of mitochondrial integrity and for OXPHOS. In general, mitochondrial-encoded transcripts showed minimal and heterogeneous increase in their levels compared with nuclear-encoded transcripts, demonstrating a preferential initial targeting of nuclear DNA. This is reminiscent of our previous data showing that DOX accumulates rapidly in the nucleus (Sardao *et al.*, 2009). Although the number of commercially available antibodies which worked in our setup was much lower than the total number of transcripts, we performed a similar analysis at

the protein level, with at least one protein from each complex, semiquantified by western blotting. No protein differences were found between saline and DOX-treated groups regardless of the analyzed tissue. This could be due to higher turnover rates for mitochondrial proteins in rodents (Brunner and Neupert, 1968; Miwa *et al.*, 2008). Therefore, neither a direct correlation can be performed, nor treatment-related differences can be properly attributed through this analytic methodology.

We complemented the study with an alternative strategy to analyze mRNA and protein data. From the PCA analysis, we obtained a consistent separation between treatment groups in the heart for all 4 respiratory complexes, suggesting that the effect of the DOX administration is clearly detected in this tissue. The boundary is particularly well defined when analyzing complex I which was previously indicated as being inhibited in DOX-induced cardiotoxicity (Santos *et al.*, 2002). As for the other tissues, clear separations occur just in specific complexes: in liver there is a clear separation in complex II, whereas in kidney clear boundaries are visible in complexes II and III. This differential response of DOX suggests that the impact of treatment

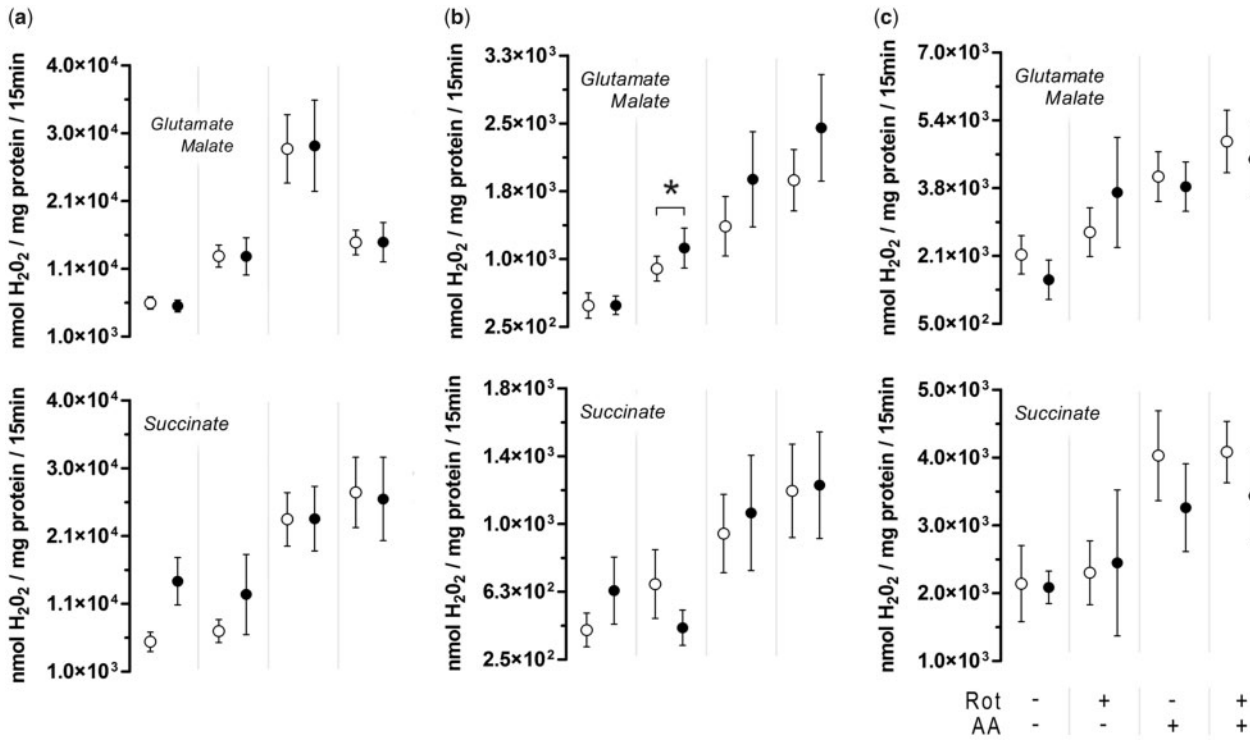


Figure 3. Effects of DOX treatment on mitochondrial H<sub>2</sub>O<sub>2</sub> production. After 15 min, endpoint H<sub>2</sub>O<sub>2</sub> levels were measured fluorimetrically through reaction with homovalinic acid. a, Heart; b, liver; c, kidney. Circles represent means of treatment groups (saline in white circles; DOX in black circles) with SEM (error bars are smaller than symbols when not visible). Differences between means of treatment were evaluated by matched pairs Student's t-test to exclude the variability related to mitochondrial. \*p < .05 versus saline group of the same model. n = 8, 7, and 6 (heart, liver, and kidney, respectively).

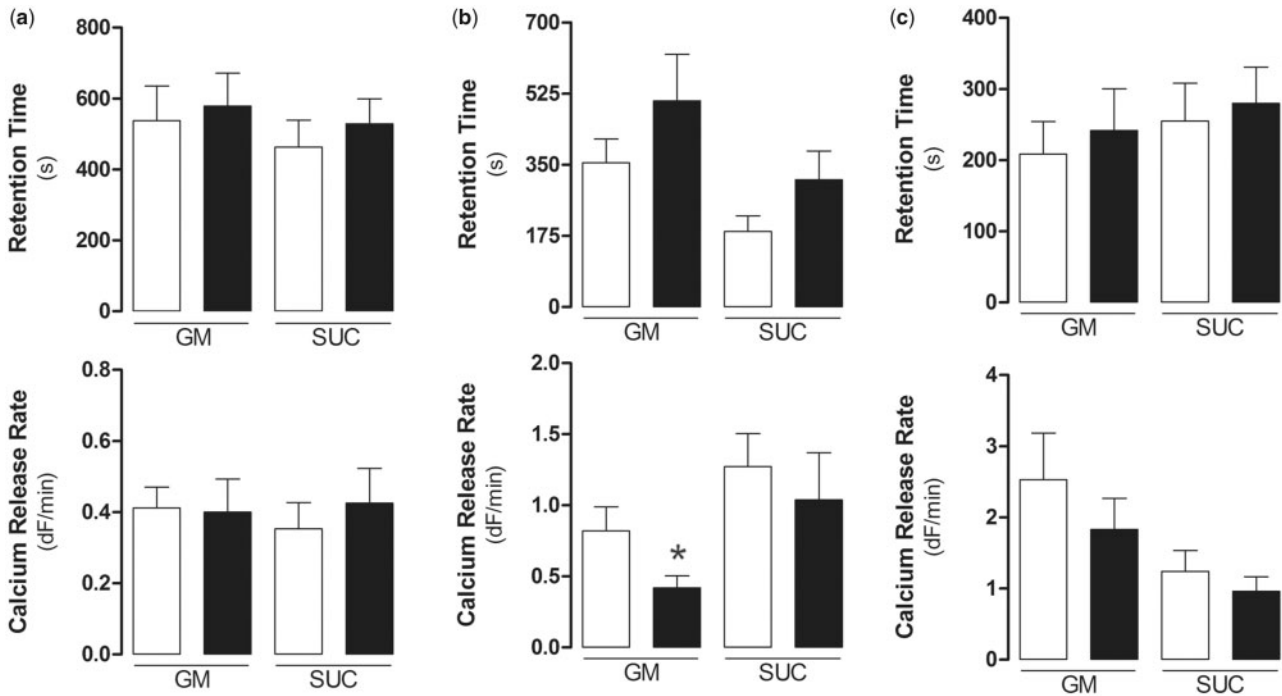
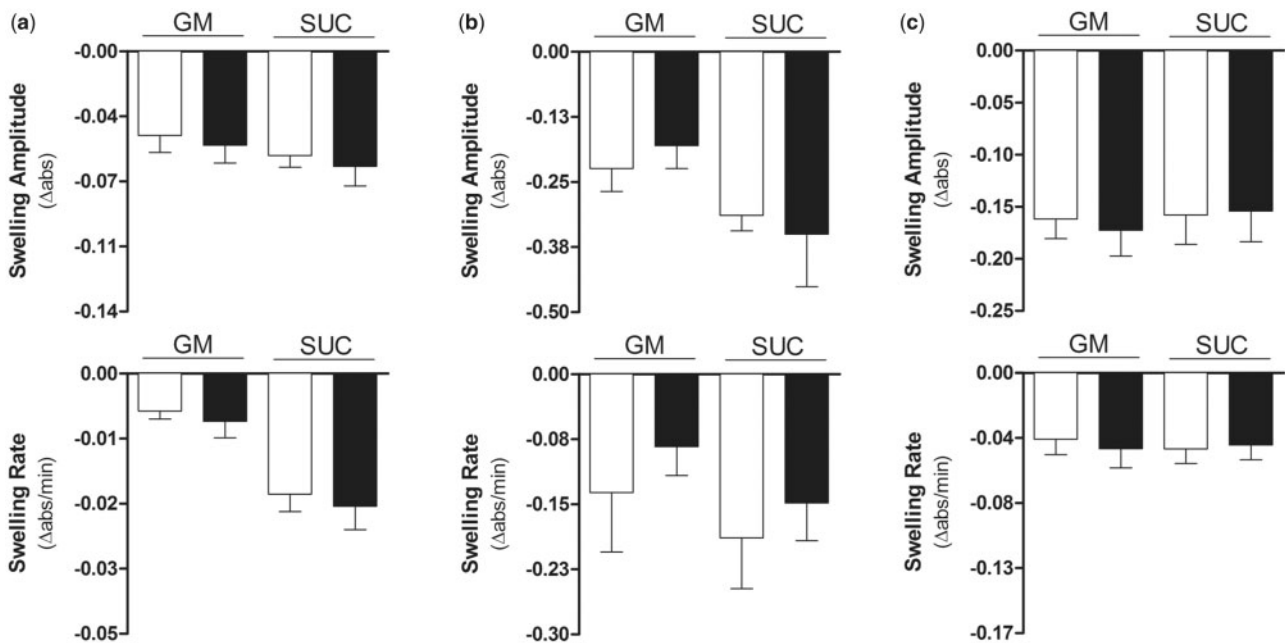


Figure 4. Effects of DOX treatment on mitochondrial calcium-loading capacity. Ca<sup>2+</sup> movements were evaluated using the extramitochondrial fluorescent probe Ca5GN after addition of a single pulse of Ca<sup>2+</sup>. The retention time is defined by the time interval between the influx and efflux of Ca<sup>2+</sup> whose fluorescence value equals the peak half-height fluorescence upon addition of calcium (larger values mean less sensitivity to mPTP). a, Heart; b, liver; c, kidney. Bars represent means of treatment groups (saline in white bars; DOX in black bars) with SEM. Differences between means of treatment groups were evaluated by matched pairs Student's t-test to exclude the variability related to mitochondrial isolation. \*p < .05 versus saline group. n = 10, 9, and 10 (heart, liver, and kidney, respectively). GM, glutamate/malate; SUC, succinate.

**Table 1.** Effect of Cyclosporin A (CsA) on Calcium-induced mPTP Evaluated With Ca5GN

Substrate	Treat.	Heart		Liver		Kidney	
		Diff. means	Pooled SE	Diff. means	Pooled SE	Diff. means	Pooled SE
		% of inhibition					
		$n_{CsA} = 4$		$n_{CsA} = 6$		$n_{CsA} = 5$	
Glutamate/malate	Saline	85.9**	25.0	107.0***	21.0	98.8***	17.0
	DOX	96.4**	24.6	101.0***	22.0	96.0**	24.4
Succinate	Saline	92.2*	37.2	72.6***	11.7	101.4**	23.7
	DOX	97.0*	39.6	100.0*	32.0	98.5**	21.9

Tabulated values represent the difference between means of groups in the absence of CsA and groups with CsA, eg, saline-glutamate/malate versus saline-glutamate/malate + CsA, and are expressed as relative percentage to the group without CsA. \* $p \leq .05$ ; \*\* $p \leq .01$ ; and \*\*\* $p \leq .001$  versus group with CsA, as evaluated by an unpaired Student's t-test. Abbreviations: Exp., experimental setup; Treat., treatment; Diff. means, difference between group means; Pooled SE, pooled standard error; nCsA, replicates number in CsA group.



**Figure 5.** Effects of DOX treatment on calcium-induced mitochondrial swelling. Mitochondrial swelling was evaluated by following the decrease in apparent absorbance of the mitochondrial suspension at 540 nm after addition of a single pulse of  $Ca^{2+}$ . The swelling amplitude presented in the graphs is defined as the difference in absorbance between the point which corresponds to half of the maximum swelling amplitude of the control record and the maximum absorbance before calcium addition (larger values mean greater sensitivity to mPTP). a, heart; b, liver; c, kidney. Bars represent means of treatment groups (saline in white bars; DOX in black bars) with SEM. Differences between means of treatment groups were evaluated by matched pairs Student's t-test to exclude the variability related to mitochondrial isolation.  $n = 10, 9,$  and  $10$  (heart, liver, and kidney, respectively). GM, glutamate/malate; SUC, succinate.

**Table 2.** Effect of CsA on Calcium-induced Mitochondrial Swelling

Substrate	Treat.	Heart		Liver		Kidney	
		Diff. means	Pooled SE	Diff. means	Pooled SE	Diff. means	Pooled SE
		% of inhibition					
		$n_{CsA} = 4$		$n_{CsA} = 6$		$n_{CsA} = 5$	
Glutamate/malate	Saline	80.6*	34.8	108.6***	24.8	87.0**	23.6
	DOX	76.6**	33.7	80.9**	22.2	90.7**	25.3
Succinate	Saline	91.6***	14.4	99.0***	38.3	88.0**	18.9
	DOX	93.8**	28.7	98.1*	29.3	87.3**	20.5

Tabulated values represent the difference between means of groups in the absence of CsA and groups with CsA, eg, saline-glutamate/malate versus saline-glutamate/malate + CsA, and are expressed as relative percentage to the group without CsA. \* $p \leq .05$ ; \*\* $p \leq .01$ ; and \*\*\* $p \leq .001$  versus group with CsA, as evaluated by an unpaired Student's t-test. Abbreviations: Exp., experimental setup; Treat., treatment; Diff. means, difference between group means; Pooled SE, pooled standard error; nCsA, replicates number in CsA group.

can be easily distinguished between the cardiac and other tissues such as the liver or kidney. Contrary to the absence or minimal changes in cardiac mitochondrial function (mPTP sensitivity, H<sub>2</sub>O<sub>2</sub> production and, respiration and oxidative stress markers [Pereira et al., 2012]), the trends detected in the PCA study confirmed complex I as the most promising target to detect acute mitochondrial changes resulting from DOX-treatment in the heart. Heart accumulates DOX slowly but to a higher extent than liver (Peters et al., 1981) which could explain why DOX inhibitory effect on transcription was more easily detected in the heart, suggesting a tissue-specific concentration-dependent effect. Alternatively, these findings could be explained on the basis of tissue-specific stability of nuclear and mitochondrial-encoded mRNAs (Connor et al., 1996), being cardiac mRNAs less stable compared with the other tissues. Nonetheless, our data suggests that the observed mitochondrial molecular alterations precede changes in mitochondrial function.

FCA allowed the identification of promising features that can be used for the detection of an acute toxicity. UQCRFS1 transcript and protein levels were involved in higher correlation changes in both kidney and heart. Complex III UQCRFS1subunit has been shown to be decreased in Barth syndrome animal models (Huang et al., 2015), a pathology which is associated to the development of cardiomyopathy (Dudek and Maack, 2017). In addition to NDUFB8, NDUFS4 mRNA levels were also identified as features with high

correlation changes in heart. Recently, Piekutowska-Abramczuk et al. (2018) reported NDUFB8 as the underlying gene in childhood-onset of Leigh-like encephalomyopathy, observing decreased NDUFS4 protein levels and lower complex I activity as well. Interestingly, NDUFS4 is an accessory subunit important in complex I assembly whereas NDUFB8 is an integral structural component of complex I essential for its function (Sanchez-Caballero et al., 2016). NDUFB8 is not involved in the catalytic activity of complex I but is an essential component of the membrane-anchor required for the full assembly of complex I and contribute to the oligomerization of complex I with complexes III and IV (Wu et al., 2016). Interestingly, we have previously suggested loss of mitochondrial supercomplexes as a possible underlying event in DOX-chronic toxicity (Pereira et al., 2016).

Our results indicate that an acute DOX treatment leads to alterations in proteins and transcripts related with complexes I, III, and IV in the heart and kidney, with a special predominance for complex I. The liver tissue, on the other hand, showed minimal alterations in molecular features, although displaying positive adjustments in terms of respiration and calcium loading capacity, 2 measures of functional changes.

By using sequential PCA and FCA, we demonstrated for the first time alterations in sets of transcripts and proteins, but not in functional measurements, that might serve as potential early acute markers of cardiac-specific mitochondrial toxicity, contributing to explain the trajectory of DOX cardiac toxicity and to measure the efficacy of novel interventions aimed at minimizing DOX cardiac liabilities in anticancer treatments (Pereira et al., 2012, 2016). Nonetheless, longer resting periods after DOX-acute treatment should be studied to determine when mitochondrial functional impairments begin to be apparent in the different organs studied. Similarly, it remains to be elucidated whether these molecular markers are detectable in the circulation of DOX-treated animals or patients. Although mRNA has become a signature-based biomarker in cancer management, their use in cardiovascular medicine is still in its earlier days; however, it would prove instrumental in the early detection of DOX-induced cardiotoxicity in the clinic and could replace myocardial biopsies, an invasive procedure to detect heart diseases.

**Table 3.** Effects of DOX Treatment on Protein Content of mPTP-related Proteins

		ANT		VDAC		Cyp-D	
		Mean	SE	Mean	SE	Mean	SE
Heart	Saline	1.02	0.05	0.96	0.02	1.00	0.03
	DOX	0.97	0.08	1.04	0.05	1.01	0.02
Liver	Saline	0.97	0.08	1.00	0.10	1.00	0.07
	DOX	1.04	0.04	0.99	0.08	1.01	0.04
Kidney	Saline	1.02	0.05	0.95	0.11	1.06	0.04
	DOX	0.99	0.05	1.04	0.08	0.95	0.05

Protein levels data are presented as arbitrary units and represent densitometry analysis of western blot membranes after image acquisition. Differences between treatment group means were evaluated by matched pairs Student's t-test. Abbreviation: SE, standard error.

**Table 4.** Effects of DOX Treatment on Transcript Level of mPTP-related

Proteins		ANT1		ANT2		VDAC1		VDAC2		VDAC3	
		Mean	SE	Mean	SE	Mean	SE	Mean	SE	Mean	SE
Heart	Saline	$8.04 \times 10^{-3}$	$5.35 \times 10^{-4}$	$2.55 \times 10^{-4}$	$1.51 \times 10^{-5}$	$1.51 \times 10^{-3}$	$2.33 \times 10^{-4}$	$4.05 \times 10^{-4}$	$3.14 \times 10^{-5}$	$5.36 \times 10^{-4}$	$3.72 \times 10^{-5}$
	DOX	$4.82 \times 10^{-3}$ <sup>a</sup>	$1.94 \times 10^{-4}$	$1.87 \times 10^{-4}$ <sup>b</sup>	$1.29 \times 10^{-5}$	$9.85 \times 10^{-4}$	$7.57 \times 10^{-5}$	$2.96 \times 10^{-4}$	$1.32 \times 10^{-5}$	$4.57 \times 10^{-4}$	$2.42 \times 10^{-5}$
Liver	Saline	$1.96 \times 10^{-4}$	$1.54 \times 10^{-5}$	$1.08 \times 10^{-3}$	$6.41 \times 10^{-5}$	$2.33 \times 10^{-3}$	$2.54 \times 10^{-3}$	$3.05 \times 10^{-4}$	$4.19 \times 10^{-5}$	$8.57 \times 10^{-4}$	$8.97 \times 10^{-4}$
	DOX	$2.00 \times 10^{-4}$	$1.03 \times 10^{-5}$	$1.12 \times 10^{-3}$	$8.38 \times 10^{-5}$	$3.23 \times 10^{-4}$	$2.32 \times 10^{-4}$	$3.01 \times 10^{-4}$	$2.10 \times 10^{-5}$	$1.28 \times 10^{-4}$	$5.98 \times 10^{-5}$
Kidney	Saline	$2.36 \times 10^{-3}$	$2.01 \times 10^{-4}$	$5.18 \times 10^{-3}$	$4.70 \times 10^{-4}$	$5.77 \times 10^{-4}$	$7.36 \times 10^{-5}$	$1.32 \times 10^{-4}$	$1.26 \times 10^{-4}$	$1.85 \times 10^{-4}$	$2.29 \times 10^{-5}$
	DOX	$2.63 \times 10^{-3}$	$2.45 \times 10^{-4}$	$5.90 \times 10^{-3}$	$4.53 \times 10^{-4}$	$4.32 \times 10^{-4}$	$8.80 \times 10^{-5}$	$1.38 \times 10^{-5}$	$1.12 \times 10^{-5}$	$1.97 \times 10^{-4}$	$2.25 \times 10^{-5}$

Total mRNA was extracted from each tissue and transcript levels were analyzed through RT-qPCR with the transcript copy number being thereafter normalized to 18S copy number. Values are shown as transcript copy number/18S copy number. For statistical analysis, tabulated values were log transformed and differences in fold-change of each tissue were detected by a 2-way ANOVA with planned contrasts and adjusted for multiple comparisons through the Sidak test. <sup>a</sup> $p \leq .05$  Saline-DOX fold-change in heart versus liver and Saline-DOX fold-change in heart versus kidney; <sup>b</sup> $p \leq .05$  Saline-DOX fold-change in heart versus kidney.  $n = 6$  for all tissues and both experimental setups. Abbreviation: SE, standard error.

## SUPPLEMENTARY DATA

Supplementary data are available at Toxicological Sciences online.

## DECLARATION OF CONFLICTING INTERESTS

The authors declared no potential conflicts of interest with respect to the research, authorship, and/or publication of this article.

## ACKNOWLEDGMENTS

This work was supported by FEDER funds through the Operational Programme Competitiveness Factors—COMPETE and national funds by FCT—Foundation for Science and Technology under the projects PTDC/DTP-FTO/1180/2012, POCI-01-0145-FEDER-007440, PTDC/DTP-FTO/2433/2014, POCI-01-0145-FEDER-016659, and POCI-01-0145-FEDER-029297. The FCT also supported doctoral fellowships for G.C.P. (SFRH/BD/36938/2007) and the post doctoral fellowship for S.P.P. (SFRH/BPD/116061/2016).

## ETHICAL APPROVAL

All applicable international, national, and/or institutional guidelines for the care and use of animals were followed. All procedures performed in animal studies were in accordance with the ethical standards of the CNC – Center for Neuroscience and Cell Biology and Medical School of the University of Coimbra.

## REFERENCES

- Ascensao, A., Ferreira, R., Oliveira, P. J., and Magalhaes, J. (2006). Effects of endurance training and acute Doxorubicin treatment on rat heart mitochondrial alterations induced by in vitro anoxia-reoxygenation. *Cardiovasc. Toxicol.* **6**, 159–172.
- Ascensao, A., Lumini-Oliveira, J., Machado, N. G., Ferreira, R. M., Goncalves, I. O., Moreira, A. C., Marques, F., Sardao, V. A., Oliveira, P. J., and Magalhaes, J. (2011). Acute exercise protects against calcium-induced cardiac mitochondrial permeability transition pore opening in doxorubicin-treated rats. *Clin. Sci. (Lond.)* **120**, 37–49.
- Ascensao, A., Magalhaes, J., Soares, J. M., Ferreira, R., Neuparth, M. J., Marques, F., Oliveira, P. J., and Duarte, J. A. (2005). Moderate endurance training prevents doxorubicin-induced in vivo mitochondriopathy and reduces the development of cardiac apoptosis. *Am. J. Physiol. Heart Circ. Physiol.* **289**, H722–H731.
- Ascensao, A., Oliveira, P. J., and Magalhaes, J. (2012). Exercise as a beneficial adjunct therapy during Doxorubicin treatment – role of mitochondria in cardioprotection. *Int. J. Cardiol.* **156**, 4–10.
- Asensio-Lopez, M. C., Soler, F., Sanchez-Mas, J., Pascual-Figal, D., Fernandez-Belda, F., and Lax, A. (2016). Early oxidative damage induced by doxorubicin: Source of production, protection by GKT137831 and effect on Ca(2+) transporters in HL-1 cardiomyocytes. *Arch. Biochem. Biophys.* **594**, 26–36.
- Barja, G. (2002). The quantitative measurement of H2O2 generation in isolated mitochondria. *J. Bioenerg. Biomembr.* **34**, 227–233.
- Broekemeier, K. M., Dempsey, M. E., and Pfeiffer, D. R. (1989). Cyclosporin A is a potent inhibitor of the inner membrane permeability transition in liver mitochondria. *J. Biol. Chem.* **264**, 7826–7830.
- Brunner, G., and Neupert, W. (1968). Turnover of outer and inner membrane proteins of rat liver mitochondria. *FEBS Lett.* **1**, 153–155.
- Cappetta, D., De Angelis, A., Sapio, L., Prezioso, L., Illiano, M., Quaini, F., Rossi, F., Berrino, L., Naviglio, S., and Urbanek, K. (2017). Oxidative stress and cellular response to doxorubicin: A common factor in the complex milieu of anthracycline cardiotoxicity. *Oxid. Med. Cell Longev.* **2017**, 1521020.
- Chatterjee, K., Zhang, J., Honbo, N., and Karliner, J. S. (2010). Doxorubicin cardiomyopathy. *Cardiology* **115**, 155–162.
- Childs, A. C., Phaneuf, S. L., Dirks, A. J., Phillips, T., and Leeuwenburgh, C. (2002). Doxorubicin treatment in vivo causes cytochrome C release and cardiomyocyte apoptosis, as well as increased mitochondrial efficiency, superoxide dismutase activity, and Bcl-2: Bax ratio. *Cancer Res.* **62**, 4592–4598.
- Connor, M. K., Takahashi, M., and Hood, D. A. (1996). Tissue-specific stability of nuclear- and mitochondrially encoded mRNAs. *Arch. Biochem. Biophys.* **333**, 103–108.
- Cunha-Oliveira, T., Ferreira, L. L., Coelho, A. R., Deus, C. M., and Oliveira, P. J. (2018). Doxorubicin triggers bioenergetic failure and p53 activation in mouse stem cell-derived cardiomyocytes. *Toxicol. Appl. Pharmacol.* **348**, 1–13.
- Davies, K. J., and Doroshov, J. H. (1986). Redox cycling of anthracyclines by cardiac mitochondria. I. Anthracycline radical formation by NADH dehydrogenase. *J. Biol. Chem.* **261**, 3060–3067.
- Demsar, J., Curk, T., Erjavec, A., Gorup C, Hocevar, T., Milutinovic, M., Mozina, M., Polajnar, M., Toplak, M., Staric, A., et al (2013). Orange: Data mining toolbox in python. *J. Mach. Learn. Res.* **14**, 2349–2353.
- Dudek, J., and Maack, C. (2017). Barth syndrome cardiomyopathy. *Cardiovasc. Res.* **113**, 399–410.
- Fabian Pedregosa, G. V., Gramfort, A., Michel, V., Thirion, B., Grisel, O., Blondel, M., Prettenhofer, P., Weiss, R., Dubourg, V., Vanderplas, J., et al. (2011). Scikit-learn: Machine learning in python. *J. Mach. Learn. Res.* **12**, 2825–2830.
- Fontaine, E., Eriksson, O., Ichas, F., and Bernardi, P. (1998). Regulation of the permeability transition pore in skeletal muscle mitochondria. Modulation By electron flow through the respiratory chain complex. *J. Biol. Chem.* **273**, 12662–12668.
- Halestrap, A. P., and Davidson, A. M. (1990). Inhibition of Ca2(+)-induced large-amplitude swelling of liver and heart mitochondria by cyclosporin is probably caused by the inhibitor binding to mitochondrial-matrix peptidyl-prolyl cis-trans isomerase and preventing it interacting with the adenine nucleotide translocase. *Biochem. J.* **268**, 153–160.
- Hayward, R., and Hydock, D. S. (2007). Doxorubicin cardiotoxicity in the rat: An in vivo characterization. *J. Am. Assoc. Lab. Anim. Sci.* **46**, 20–32.
- Huang, Y., Powers, C., Madala, S. K., Greis, K. D., Haffey, W. D., Towbin, J. A., Purevjav, E., Javadov, S., Strauss, A. W., and Khuchua, Z. (2015). Cardiac metabolic pathways affected in the mouse model of barth syndrome. *PLoS One* **10**, e0128561.
- Hunter, J. D. (2007). Matplotlib: A 2D graphics environment. *Comput. Sci. Eng.* **9**, 90–95.
- Jones, E., Oliphant, T., and Peterson, P. (2001). SciPy: Open source scientific tools for python. Available at: <http://scipy.org>
- McKinney, W. (2010). Data structures for statistical computing in python, Vol. 445, pp. 51–56.

- Miwa, S., Lawless, C., and von Zglinicki, T. (2008). Mitochondrial turnover in liver is fast in vivo and is accelerated by dietary restriction: Application of a simple dynamic model. *Aging Cell* 7, 920–923.
- Nair, A. B., and Jacob, S. (2016). A simple practice guide for dose conversion between animals and human. *J. Basic Clin. Pharm.* 7, 27–31.
- Oliveira, P. J., Bjork, J. A., Santos, M. S., Leino, R. L., Froberg, M. K., Moreno, A. J., and Wallace, K. B. (2004). Carvedilol-mediated antioxidant protection against doxorubicin-induced cardiac mitochondrial toxicity. *Toxicol. Appl. Pharmacol.* 200, 159–168.
- Oliveira, P. J., Santos, M. S., and Wallace, K. B. (2006). Doxorubicin-induced thiol-dependent alteration of cardiac mitochondrial permeability transition and respiration. *Biochemistry (Mosc)* 71, 194–199.
- Pereira, G. C., Pereira, S. P., Pereira, C. V., Lumini, J. A., Magalhaes, J., Ascensao, A., Santos, M. S., Moreno, A. J., and Oliveira, P. J. (2012). Mitochondrionopathy phenotype in doxorubicin-treated Wistar rats depends on treatment protocol and is cardiac-specific. *PLoS One* 7, e38867.
- Pereira, G. C., Pereira, S. P., Tavares, L. C., Carvalho, F. S., Magalhaes-Novais, S., Barbosa, I. A., Santos, M. S., Bjork, J., Moreno, A. J., Wallace, K. B., et al. (2016). Cardiac cytochrome c and cardiolipin depletion during anthracycline-induced chronic depression of mitochondrial function. *Mitochondrion* 30, 95–104.
- Pereira, G. C., Silva, A. M., Diogo, C. V., Carvalho, F. S., Monteiro, P., and Oliveira, P. J. (2011). Drug-induced cardiac mitochondrial toxicity and protection: From doxorubicin to carvedilol. *Curr. Pharm. Des.* 17, 2113–2129.
- Peters, J. H., Gordon, G. R., Kashiwase, D., and Acton, E. M. (1981). Tissue distribution of doxorubicin and doxorubicinol in rats receiving multiple doses of doxorubicin. *Cancer Chemother. Pharmacol.* 7, 65–69.
- Piekutowska-Abramczuk, D., Assouline, Z., Mataković, L., Feichtinger, R. G., Koňáriková, E., Jurkiewicz, E., Stawiński, P., Gusic, M., Koller, A., Pollak, A., et al. (2018). NDUF8 mutations cause mitochondrial complex I deficiency in individuals with leigh-like encephalomyopathy. *Am. J. Hum. Genet.* 102, 460–467.
- Rajdev, S., and Reynolds, I. J. (1993). Calcium green-5N, a novel fluorescent probe for monitoring high intracellular free Ca<sup>2+</sup> concentrations associated with glutamate excitotoxicity in cultured rat brain neurons. *Neurosci. Lett.* 162, 149–152.
- Sanchez-Caballero, L., Guerrero-Castillo, S., and Nijtmans, L. (2016). Unraveling the complexity of mitochondrial complex I assembly: A dynamic process. *Biochim. Biophys. Acta* 1857, 980–990.
- Santos, D. L., Moreno, A. J., Leino, R. L., Froberg, M. K., and Wallace, K. B. (2002). Carvedilol protects against doxorubicin-induced mitochondrial cardiomyopathy. *Toxicol. Appl. Pharmacol.* 185, 218–227.
- Sardao, V. A., Oliveira, P. J., Holy, J., Oliveira, C. R., and Wallace, K. B. (2009). Doxorubicin-induced mitochondrial dysfunction is secondary to nuclear p53 activation in H9c2 cardiomyoblasts. *Cancer Chemother. Pharmacol.* 64, 811–827.
- Silva, F. S. G., Costa, C. F., Marques, R. J., Oliveira, P. J., and Pereira, G. C. (2018). Pharmacological targeting of the mitochondrial permeability transition pore for cardioprotection. In *Mitochondrial biology and experimental therapeutics* (P. J. Oliveira, Ed.), pp. 423–490. Springer International Publishing, Cham.
- Simunek, T., Sterba, M., Popelova, O., Adamcova, M., Hrdina, R., and Gersl, V. (2009). Anthracycline-induced cardiotoxicity: Overview of studies examining the roles of oxidative stress and free cellular iron. *Pharmacol. Rep.* 61, 154–171.
- Singal, P. K., and Iliskovic, N. (1998). Doxorubicin-induced cardiomyopathy. *N. Engl. J. Med.* 339, 900–905.
- Solem, L. E., Heller, L. J., and Wallace, K. B. (1996). Dose-dependent increase in sensitivity to calcium-induced mitochondrial dysfunction and cardiomyocyte cell injury by doxorubicin. *J. Mol. Cell. Cardiol.* 28, 1023–1032.
- Steinherz, L. J., Steinherz, P. G., Tan, C. T., Heller, G., and Murphy, M. L. (1991). Cardiac toxicity 4 to 20 years after completing anthracycline therapy. *JAMA* 266, 1672.
- Sterba, M., Popelova, O., Vavrova, A., Jirkovsky, E., Kovarikova, P., Gersl, V., and Simunek, T. (2013). Oxidative stress, redox signaling, and metal chelation in anthracycline cardiotoxicity and pharmacological cardioprotection. *Antioxid. Redox Signal.* 18, 899–929.
- Tokarska-Schlattner, M., Zaugg, M., Zuppinger, C., Wallimann, T., and Schlattner, U. (2006). New insights into doxorubicin-induced cardiotoxicity: The critical role of cellular energetics. *J. Mol. Cell. Cardiol.* 41, 389–405.
- van Dalen, E. C., Raphael, M. F., Caron, H. N., and Kremer, L. C. (2009). Treatment including anthracyclines versus treatment not including anthracyclines for childhood cancer. *Cochrane Database Syst. Rev.* doi: 10.1002/14651858.CD006647.pub2(1), CD006647. Available at: <https://www.cochranelibrary.com/cdsr/doi/10.1002/14651858.CD006647.pub2/full>
- Wallace, K. B. (1986). Nonenzymatic oxygen activation and stimulation of lipid peroxidation by doxorubicin-copper. *Toxicol. Appl. Pharmacol.* 86, 69–79.
- Wallace, K. B. (2007). Adriamycin-induced interference with cardiac mitochondrial calcium homeostasis. *Cardiovasc. Toxicol.* 7, 101–107.
- Wu, M., Gu, J., Guo, R., Huang, Y., and Yang, M. (2016). Structure of mammalian respiratory supercomplex I1III2IV1. *Cell* 167, 1598–1609.e10.
- Zhou, S., Heller, L. J., and Wallace, K. B. (2001). Interference with calcium-dependent mitochondrial bioenergetics in cardiac myocytes isolated from doxorubicin-treated rats. *Toxicol. Appl. Pharmacol.* 175, 60–67.
- Zhou, S., Palmeira, C. M., and Wallace, K. B. (2001). Doxorubicin-induced persistent oxidative stress to cardiac myocytes. *Toxicol. Lett.* 121, 151–157.
- Zhou, S., Starkov, A., Froberg, M. K., Leino, R. L., and Wallace, K. B. (2001c). Cumulative and irreversible cardiac mitochondrial dysfunction induced by doxorubicin. *Cancer Res.* 61, 771–777.